https://doi.org/10.5194/egusphere-2024-3719
Preprint. Discussion started: 13 December 2024

Hemispheric differences in ozone across the stratosphere-troposphere exchange region

Rodrigo J. Seguel [1, 2], Charlie Opazo [1, 2], Yann Cohen [3], Owen R. Cooper [4], Laura Gallardo [1, 2], Björn-Martin Sinnhuber [5], Florian Obersteiner [5], Andreas Zahn [5], Peter Hoor [6], Susanne Rohs [7]

[1]Center for Climate and Resilience Research (CR)[2], Santiago, Chile
[2]Department of Geophysics, Faculty of Physical and Mathematical Sciences, University of Chile, Santiago, Chile
[3]Institut Pierre-Simon Laplace (IPSL), Sorbonne Université/CNRS, Paris, France
[4]NOAA Chemical Sciences Laboratory, Boulder, USA
[5]Karlsruhe Institute of Technology, Institute of Meteorology and Climate Research (IMK), Karlsruhe, Germany
[6]Institute for Atmospheric Physics, Johannes Gutenberg-University, Mainz, Germany
[7]Institute of Energy and Climate Systems 3 – Troposphere (ICE-3), Forschungszentrum Jülich, Jülich, Germany

Correspondence to: Rodrigo J. Seguel (rodrigoseguel@uchile.cl)

Abstract

This study examined the ozone mixing ratios in the upper troposphere-lower stratosphere (UTLS) to determine whether the ozone levels in the lowermost stratosphere are lower in the Southern (SH) than in the Northern Hemisphere (NH), as suggested by total column ozone observations. We utilized unique in situ measurements from the High Altitude and Long Range (HALO) research aircraft deployed over the southernmost region of South America (45-60 ºS) in September-November 2019 as a part of the Southern Hemisphere Transport, Dynamics, and Chemistry (SouthTRAC) research campaign. In addition, the mission period enabled us to examine the impact of an early stratospheric sudden warming (SSW) event, which triggered a breakdown of the southern polar vortex in September 2019. In situ measurements from IAGOS commercial aircraft (45-60 ºN), ozonesondes (Patagonia) and CAMS reanalysis data were considered for comparative analysis. Stratospheric air was identified using relative humidity (<20%) and carbon monoxide (<50 nmol mol^{-1}) thresholds. Our results show that air masses of stratospheric origin had higher ozone abundances in the NH UTLS than in the SH (between 300-200 hPa and 45-60° latitude). In high ozone depletion years in the stratospheric vortex, the SH ozone median (170 nmol mol^{-1}) was only 51% of that in the NH (330 nmol mol^{-1}), while in low depletion years, SH ozone median (210 nmol mol^{-1}) reached 57% of the NH values (370 nmol mol^{-1}). Notably, the SSW event increased SH UTLS by 37% (46 nmol mol^{-1}) during the SouthTRAC mission compared to high depletion years.

https://doi.org/10.5194/egusphere-2024-3719
Preprint. Discussion started: 13 December 2024

1 Introduction

Ozone (O_3) has generated an effective radiative forcing (ERF) of +0.47 [0.24 to 0.71] W m^{-2} over the industrial era, from 1750 to 2019. The ERF for ozone represents 17% of the total anthropogenic ERF change, estimated at +2.72 [1.96 to 3.48] W m^{-2} (Forster et al, 2021). The ozone abundance in the troposphere is related to the atmosphere's oxidizing capacity and is closely associated with methane abundance, the second strongest greenhouse gas, due to hydroxyl radical (·OH) reactions (Saunois et al., 2020). At ground level, short-term exposure to ozone impairs human lung function and contributes to developing asthma symptoms in susceptible people (McConnell et al., 2002; Zheng et al., 2021). Total global mortality due to long-term ozone exposure has been estimated at 365,000 [175,000 to 564,000] deaths in 2019 (Health Effects Institute, 2020).

The tropospheric ozone budget is controlled by chemical production and loss, dry deposition and stratosphere-troposphere exchange (STE) (Archibald et al., 2020). Oxidations of volatile organic compounds (VOC) initiated by hydroxyl radicals lead to tropospheric ozone formation. During this process, hydroperoxyl (HO_2) and alkyl peroxy radicals (RO_2) reactions with nitric oxide (NO) yield nitrogen dioxide (NO_2), which photolyzes to produce O_3 (Monks et al., 2015). In the troposphere, the chemical loss results mainly from ozone photolysis ($\lambda \leq 320$ nm) and ozone reaction with hydroxyl and hydroperoxyl radicals (Atkinson, 2000). An important ozone sink is dry deposition at the surface (Clifton et al., 2020).

The STE, estimated at 284 ±193 Tg O_3 $year^{-1}$ (Griffiths et al., 2021; Szopa et al., 2021), is comparable with the net chemical ozone production in the troposphere. STE involves several mechanisms, including tropopause folds within mid-latitude cyclones, cutoff-low decay and gravity wave breaking (Archibald et al., 2020; Cooper et al., 2004; Stohl et al., 2003). STE shows strong geographical asymmetry and seasonal cycles. STE dominates in the extratropics, with hotspots in mountain regions of North and South America, over the Tibetan Plateau and in the storm tracks over the North Atlantic Ocean and North Pacific Ocean, which are more intense in winter and early spring in both hemispheres (Škerlak et al., 2014).

The poleward expansion of the SH Hadley circulation has also been proposed as a mechanism able to enhance downward transport of ozone from the stratosphere to the troposphere at higher latitudes (Lu et al., 2019). STE's contribution to the tropospheric ozone budget is expected to increase due to declining levels of ozone-depleting substances (ODS) and the Brewer-Dobson circulation (BDC) acceleration, especially in the lower stratosphere, caused by increasing greenhouse gas emissions (Butchart, 2014). In contrast, simulations based on climate models do not show BDC acceleration in the mid-stratosphere of the mid-latitude NH since the late 1980s due to declining ODS and the timing of volcanic eruptions (Garfinkel et al., 2017).

Ozone changes in the upper troposphere-lower stratosphere (UTLS) strongly impact the radiative forcing of the atmosphere (Riese et al., 2012; Skeie et al., 2020). Therefore, in situ measurements in the UTLS, characterized by bidirectional trace gas exchange (Gettelman et al., 2011), are crucial to reducing the uncertainty of chemical climate models and validating satellite retrievals (Bourgeois et al., 2020). Unfortunately, in the Southern Hemisphere, measurements from IAGOS (In-service Aircraft for a Global Observing System: Petzold et al., 2015) commercial aircraft rarely extend beyond 35ºS, and only a few aircraft-based research missions have characterized UTLS chemical composition in this area. The HALO (High Altitude and LOng

https://doi.org/10.5194/egusphere-2024-3719
Preprint. Discussion started: 13 December 2024

range) aircraft measured dry air masses descending from the stratosphere up to an altitude of 7 km a.s.l. over the Antarctic in September 2012 (Rolf et al., 2015). Also, flights over the South Atlantic and South Pacific Oceans conducted by the Atmospheric Tomography (ATom) mission measured a higher frequency of stratospheric intrusions during spring (Bourgeois et al., 2020). In addition, valuable long-term vertical ozone profiles have been obtained through ozonesonde launches at remote sites in higher latitudes of SH, such as the Ushuaia, Argentina and Lauder, New Zealand stations, since 2008 and 1986, respectively (Zeng et al., 2024).

In this context, the research project Southern Hemisphere Transport, Dynamics, and Chemistry (SouthTRAC) was designed to comprehensively study the dynamical and chemical processes in the SH UTLS region using the HALO instrumented aircraft during the late winter and spring seasons (September-November) of 2019 (Rapp et al., 2021). SouthTRAC coincided with intense Australian bushfires and biomass-burning events in central South America, which produced plumes detected by HALO in the UTLS (Kloss et al., 2021; Johansson et al., 2022). The mission also coincided with a polar stratospheric sudden warming (SSW) event that occurred in September 2019 (Rapp et al., 2021). SSW in SH is a phenomenon that is unusual compared with the higher frequency SSW events in the NH (Dunn et al., 2020). SSW is caused by wave events that can decelerate the westerly polar night jet and warm the polar stratosphere by descending motion, resulting in reduced heterogeneous active chlorine formation onto polar stratospheric clouds and less catalytic ozone depletion (Scambos and Stammerjohn, 2020). Accordingly, the annual mean total ozone reported in 2019 was 65 DU higher than the long-term average, at 60º-90ºS (Dunn et al., 2020).

The stratospheric ozone abundance in southern mid-and high latitudes is much less than in the NH, with this difference peaking during the springtime months when high-latitude total ozone is roughly 40% lower in the southern hemisphere (see Figure 2.63 in Dunn et al., 2023). Presumably, ozone in SH stratospheric intrusions should be proportionally less than in NH intrusions. However, confirmation of this hypothesis has been precluded due to the lack of in situ observations in the SH. Therefore, in this study, we conducted a comparative analysis of various features of the Northern and Southern Hemisphere UTLS, focusing on a latitude band where stratospheric intrusions frequently originate. The analysis relies on stratospheric and tropospheric chemical tracers measured during the SouthTRAC mission and by IAGOS commercial aircraft. Specifically, we quantified the ozone mixing ratios in air masses exhibiting stratospheric character and examined the interannual variability between years of high and low ozone depletion according to the occurrence of SSW events. In addition, by providing this characterization of ozone and chemical species exchange in the UTLS, we have identified an important data set for evaluating the models that simulate ozone transport from the stratosphere to the troposphere in both hemispheres.

2 Methodology

2.1 Region and study period

The SouthTRAC mission was conducted mainly over the southernmost region of South America within the latitudinal and meridional band 45º-60ºS and 30º-85W, respectively (**Fig. 1**). The mission had two stages: 9 Sep-6 Oct 2019 and 6-15 Nov

https://doi.org/10.5194/egusphere-2024-3719
Preprint. Discussion started: 13 December 2024

2019, totaling 16 flights, coinciding with the maximum ozone depletion in Antarctica. The UTLS portion studied ranged between 200 (~12 km) and 300 (~9 km) hPa. For comparison, IAGOS data were analyzed for the same latitudinal band and altitude range in the Northern Hemisphere. **Figure 1** shows the sampling density given by the aircraft's positional data to identify those regions of the atmosphere with more data availability. In addition, **Figure S1** in the Supplement depicts the highest number of GPS observations obtained between 300 and 200 hPa compared to the range of 700 to 300 hPa.

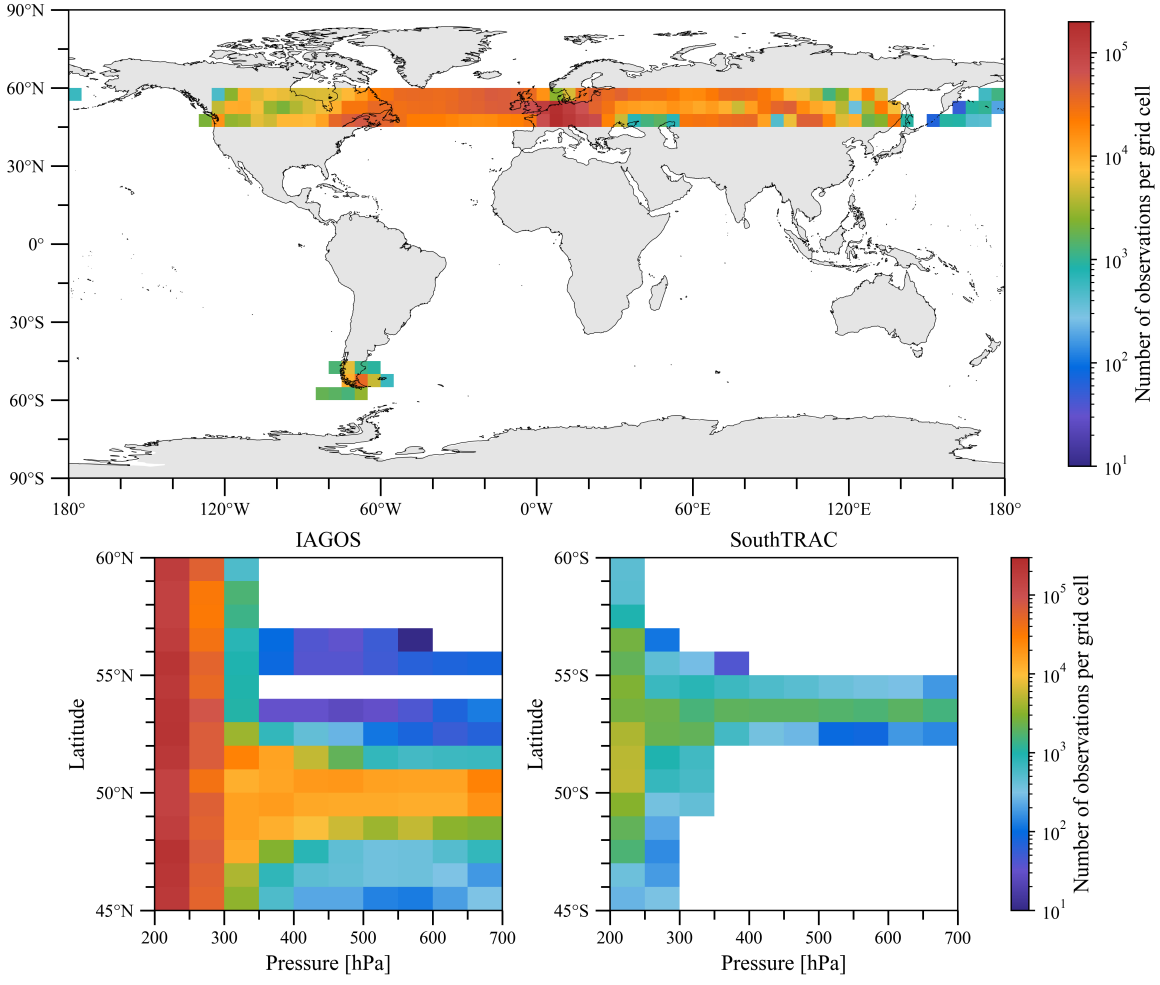

Figure 1: Routes position frequency obtained from aircraft GPSs. All panels show only SouthTRAC and IAGOS data within the same latitudinal band 45º-60º in the SH and NH. The upper panel shows the number of GPS observations by grid cell (5º x 5º) between 700 and 200 hPa. The lower panels show the number of GPS observations in every grid cell (1º x 50 hPa) between 700 and 200 hPa for IAGOS (left) and SouthTRAC (right).

Furthermore, we distinguished the interannual variability of every hemispheric considering low-depletion years (defined in this research as years disrupted by SSW) from high-depletion years (**Table 1**). Additionally, given that the ozone-depleted air masses typically reach their minimum ozone content in October (March) of the Southern (Northern) hemisphere, we split the

https://doi.org/10.5194/egusphere-2024-3719
Preprint. Discussion started: 13 December 2024

flights into late winter-early spring and mid-spring, representing the latter, the period when depleted ozone air likely reaches the SouthTRAC study region.

Table 1: Study period considered for both hemispheres, including late winter-early spring and mid-spring subperiods. Low and high ozone depletion years in terms of SSW are also indicated.

Hemisphere (lat., lon.)	Study period (no. flights)	Late winter-early spring (no. flights)	Mid spring (no. flights)	low-depletion years (data source)	High-depletion years (data source)	Number of measurements
NH (45°N-60°N, 180°E-180°W)	4 Mar - 20 May (1291)	4 - 31 Mar (456)	1 Apr – 20 May (835)	2018, 2019, 2021 & 2022 (IAGOS)	2011 & 2020 (IAGOS)	Pressure: 4097k O_3: 2068k CO: 2371k H_2O: 1788k RHL: 1929k
SH (45°S-60°S, 30°W-85°W)	4 Sep - 20 Nov (16)	4 - 30 Sep (10 flights)	1 Oct - 20 Nov (6 flights)	2019 (SouthTRAC)	2008-2018 (WOUDC)	Pressure: 67k O_3: 61k CO: 42k H_2O: 67k RHL: 67k

2.2 SouthTRAC measurements

During the SouthTRAC mission, the HALO aircraft was equipped with 13 instruments for sampling the physical and chemical properties of the atmosphere. This research focuses on the measurements of ozone, carbon monoxide (CO), water vapor, nitric acid (HNO_3) and hydrogen chloride (HCl).

In situ ozone was measured by the Fast AIRborne Ozone monitor (FAIRO) provided by the Karlsruhe Institute of Technology (KIT). FAIRO combines two measurement principles: UV ozone absorption at 255 nm and dry chemiluminescence from the reaction of O_3 with an organic dye (coumarin) at 500 nm (Ermel et al., 2013). In this dual configuration, the UV photometer calibrated the chemiluminescence response. We utilized ozone records measured by chemiluminescence due to their higher sampling frequency (5 Hz) compared with UV photometry (0.25 Hz). Typical one standard deviation (1σ) measurement precision is 0.08 nmol mol^{-1} for the UV spectrometer measuring at 0.25 Hz and ~0.05 nmol mol^{-1} for the chemiluminescence detector measuring at 5 Hz, 1 bar and 5 nmol mol^{-1} absolute mixing ratio (Zahn et al., 2012). The estimated uncertainty for UV photometer measurements was 2% and for the combined techniques (UV and chemiluminescence) was 2.5%.

The University of Mainz Airborne Quantum Cascade Laser Spectrometer (UMAQS) measured in situ carbon monoxide. This instrument is based on direct absorption in the near-infrared through a continuous-wave quantum cascade laser (Müller et al., 2015). The instrument had a typical CO precision of 0.68 nmol mol^{-1} (2σ), an accuracy of 1.2 nmol mol^{-1} and a total uncertainty of 1.4 nmol mol^{-1}.

Static pressure and static temperature were measured by Basic HALO Measurement and Sensor System (BAHAMAS) with an estimated accuracy of 0.3 hPa and 0.5 K, respectively (Giez et al., 2017; Kaufmann et al., 2018). BAHAMAS also measured water vapor at the absorption line of 1.37 µm using the Sophisticated Hygrometer for Atmospheric ResearCh (SHARC), a

https://doi.org/10.5194/egusphere-2024-3719
Preprint. Discussion started: 13 December 2024

tunable diode laser hygrometer. The limit of detection of SHARC measurement achieved during SouthTRAC campaign was 2 μmol mol^{-1} with an absolute uncertainty of ±1 μmol mol^{-1} (Kaufmann et al., 2018).

Nitric acid and hydrogen chloride were measured using the Airborne Chemical Ionization Mass Spectrometer (AIMS). In this system, the ion source generates reagent ions (SF_5^-) that selectively react with HNO_3 and HCl to form $HFNO_3^-$ and $HFCl^-$, respectively. A fast quadrupole mass spectrometer then separates the ion products based on their mass-to-charge ratio. Typical accuracy, precision (1σ), and limit of detection are 16%, 20%, and 20 pmol mol^{-1} for HNO_3 and 12%, 16%, and 15 pmol mol^{-1} for HCl, respectively (Jurkat et al., 2016).

2.3 Ozonesonde data

Ozonesondes launched between 2008 and 2018 at Ushuaia, Argentina (54.85 ºS, 68.31 ºW) were obtained from the World Ozone and Ultraviolet Radiation Data Centre, WOUDC (https://woudc.org/) aiming to compare SouthTRAC measurements with historical data. A total of 117 validated ozonesondes were linearly interpolated to an altitude grid with intervals of 50 m (Ohyama et al., 2018).

During 2008-2018, two radiosonde models were utilized. The Vaisala RS91 sensor was replaced in October 2018 by the RS41 model. The latter performs better than the older version, particularly in cloudy conditions (Jensen et al., 2016). Overall, both sensors have an uncertainty of 5% and show a consistent difference of about 1-2%, with the RH of the RS41 almost always greater than RS91 (Jensen et al., 2016).

2.4 IAGOS data set

The IAGOS research infrastructure provides in situ measurements of chemical species on board several commercial aircraft. IAGOS is a continuation of the former observation systems MOZAIC (Measurement of Ozone and Water Vapor by Airbus In-Service Aircraft: Marenco et al., 1998) and also includes the CARIBIC measurement system (Civil Aircraft for the Regular Investigation of the Atmosphere Based on an Instrument Container: (Brenninkmeijer et al., 1999, 2007; Stratmann et al., 2016), now called IAGOS-CORE and IAGOS-CARIBIC.

The MOZAIC observations started in August 1994 for ozone and water vapor on board five equipped aircraft, whereas the carbon monoxide measurements started in December 2001. The CARIBIC observations started in 1997 for a wide range of chemical species, including ozone, water vapor and CO, on a single aircraft.

IAGOS-CORE provides ozone (CO) data using an ultraviolet (infrared) absorption spectrometer, with an accuracy, precision and time response of 2 nmol mol^{-1}, 2% and 4 s (5 nmol mol^{-1}, 5%, 30 s) respectively (Nédélec et al., 2003; Nédélec et al., 2015; Thouret et al., 1998). Water vapor is measured with a capacitive hygrometer, characterized by an accuracy of 5% in RH with respect to liquid water (RHL), or 6% RHL in the vicinity of the thermal tropopause at midlatitudes, and a time response of 5 – 300 s (Helten et al., 1998; Neis et al., 2015; Rolf et al., 2024; Smit et al., 2014).

https://doi.org/10.5194/egusphere-2024-3719
Preprint. Discussion started: 13 December 2024

IAGOS-CARIBIC uses the identical instrument to measure ozone as described for HALO (see section 2.2). CO data are measured by a commercial resonance fluorescence UV instrument modified for use onboard commercial aircraft. Its accuracy, precision and time response are respectively less than 2 nmol mol^{-1}, 1 – 2 nmol mol^{-1}, and less than 2 s (Scharffe et al., 2012). Water vapor measurements are performed with a photoacoustic laser spectrometer and a frost-point hygrometer, with an accuracy of less than 4 % or 0.3 µmol mol^{-1} for the mixing ratio. The time response varies between 5 and 30 s for humid (>100 ppm) and dry air masses (<10 ppm) respectively (Dyroff et al., 2015; Zahn et al., 2014).

2.5 Water vapor thresholds

We utilized several sensors with different accuracies to filter air masses by RH. Vaisala ozonesonde sensors have a lower response time, and their vertical resolution highly depends on temperature; thus, ozonesonde sensors are less accurate than SHARC, IAGOS-CORE, and IAGOS-CARIBIC measurements. Therefore, we tested different relative humidity levels, from 50% to 10% (every 10 intervals), to effectively filter tropospheric moist mid-latitude air masses. We estimated that a RH lower than 20% is effective in excluding tropospheric air masses richer in water vapor and is sufficiently conservative, given the sensor accuracy. This threshold behaves similarly to the 50 nmol mol^{-1} CO filter (analyzed in more detail in Section 3.2).

2.6 CAMS reanalysis

We utilized vertical profiles of ozone, temperature and specific humidity from the chemical reanalysis CAMSRA (CAMS, Copernicus Atmosphere Monitoring Service, reanalysis). CAMSRA has 60 model levels from the surface to the top of the atmosphere, a horizontal resolution of 0.75°x 0.75° and a time resolution every 3 hours (Inness et al., 2019). We processed the profiles from all longitudes between 45°N-60°N and 45°S-60°S for the periods indicated in **Table 1**. We calculated the relative humidity with respect to liquid water from temperature and specific humidity and applied the same filters described in the previous section. For this comparison, we reduced the number of pressure bins between 300 and 200 hPa to 5 bins to minimize differences in the number of observations found at higher vertical resolution.

3 Results and discussion

In the following sections, we followed two principles: (1) the stratospheric air character was assigned in the UTLS according to relative humidity, and (2) the enhanced trace gases simultaneously measured, at high time resolution, on board HALO, determined the tropospheric or stratospheric origin of the air masses.

3.1 Ozone, carbon monoxide and water vapor overview

Tracer-to-tracer scatterplots between stratospheric ozone tracer and tropospheric tracers, such as water vapor and carbon monoxide at two pressure intervals, are shown in **Figures 2** and **3**. Stratospheric and tropospheric tracer scatterplots have been used in previous works to provide a magnitude of bidirectional exchange across the tropopause by the identification of

https://doi.org/10.5194/egusphere-2024-3719
Preprint. Discussion started: 13 December 2024

stratospheric and tropospheric branches and mixed air regions according to the tracer abundances (Gettelman et al., 2011).

In general, we observed higher ozone values in the UTLS and free troposphere of the NH compared to the SH. Scatterplots show that ozone between 300-200 hPa in the SH rarely exceeds 400 nmol mol^{-1}. In contrast, in the NH, high ozone levels near 1000 nmol mol^{-1} associated with low water vapor levels (i.e., drier air) are observed. The same pattern is observed between 700 and 300 hPa, with ozone levels in the NH up to twice that observed in SH (200 nmol mol^{-1}). **Figure 2** also shows that the low-depletion years in the NH tend to have higher ozone levels at low water vapor levels, compared with high-depletion years in both interval pressures.

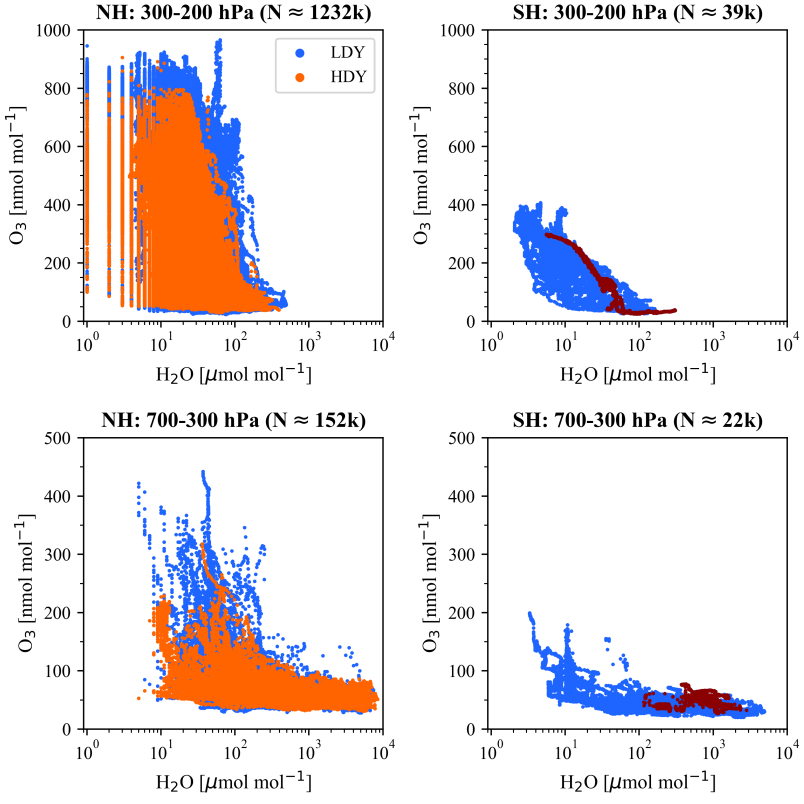

Figure 2: Scatter plots of ozone versus water vapor. The left panels show scatter plots for the NH between 300-200 and 700-300 hPa (IAGOS data set). The right panels show the same for the SH (SouthTRAC campaign). Low and high-depletion years are in blue and orange colors, respectively. Above each plot, N stands for the number of observations. In the SH, the flight conducted on 12 Nov 2019 is highlighted in dark red.

Tracer-to-tracer scatterplots of ozone and carbon monoxide show that in the NH, CO reaches higher levels (~240 nmol mol^{-1}) at both 300-200 and 700-300 hPa (**Figure 3**). Notice that some CO values are not included in NH because they were not simultaneously measured with O_3. In this regard, we found CO mixing ratios up to 319 ppb between 300-200 hPa and 325 ppb between 300-700 hPa. Low-depletion years in the NH tend to exhibit higher ozone at low CO values than high-depletion years. In contrast, in the SH, carbon monoxide rarely exceeds 100 nmol mol^{-1} in both pressure intervals (300-200 hPa and 700-300

https://doi.org/10.5194/egusphere-2024-3719
Preprint. Discussion started: 13 December 2024

hPa). An exception of this behavior was observed during the flight conducted on 12 Nov 2019 (mid-spring), which detected elevated levels of carbon monoxide (>200 nmol mol^{-1}), ozone (>100 nmol mol^{-1}) and water vapor (>100 µmol mol^{-1}) above 9 km. These elevated levels were presumably attributed to tropospheric plumes and may have been pyrogenic in origin, given the simultaneous bushfires in Australia that extended from Sep 2019 to Mar 2020 (Kloss et al., 2021).

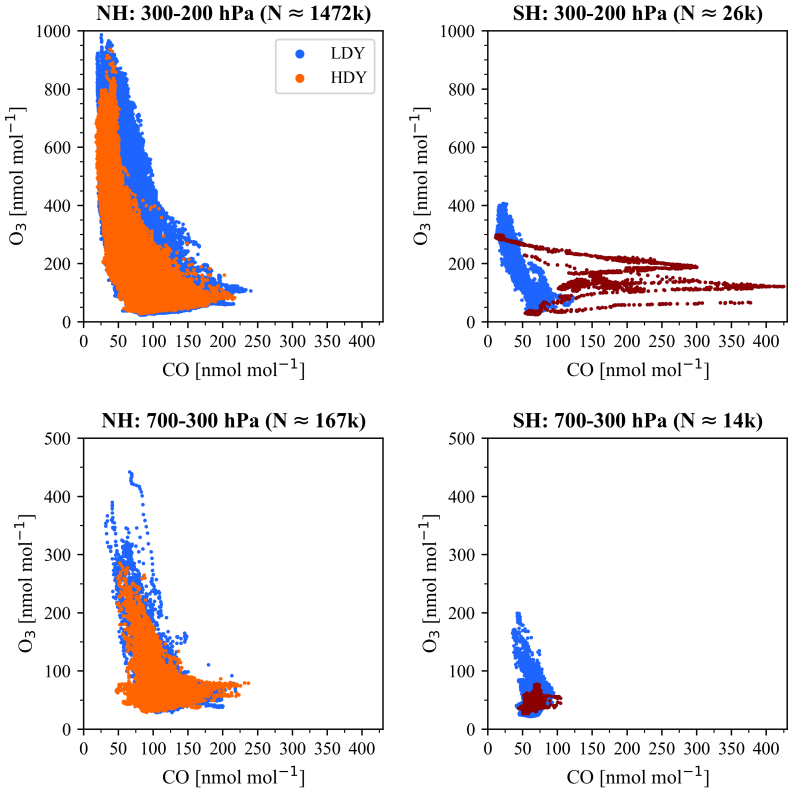

Figure 3: Scatter plots of ozone versus carbon monoxide. The left panels show scatter plots for the NH between 300-200 and 700-300 hPa (IAGOS data set). The right panels show the same for the SH (SouthTRAC campaign). Low and high-depletion years are in blue and orange colors, respectively. Above each plot, N stands for the number of observations. In the SH, the flight conducted on 12 Nov 2019 is highlighted in dark red.

In this regard, the abundance of nitric acid and hydrogen chloride are also useful in determining the plume's origin since these two species are stable in the stratosphere but more prone to removal in the troposphere. Tracer-to-tracer scatterplots of these species versus ozone and carbon monoxide (**Fig. A1**) show that nitric acid and hydrogen chloride were, in general, higher when ozone was higher and lower when carbon monoxide was higher. This anticorrelation between CO and stratospheric traces suggests that this plume predominantly originates from the troposphere. Nevertheless, we cannot entirely exclude the mixing processes of stratospheric and tropospheric air masses, as shown by the fluctuations registered during the flight (**Fig. A1**).

In summary, air masses with CO mixing ratios below 50 nmol mol^{-1} at 300-200 hPa are almost exclusively above 100 nmol

https://doi.org/10.5194/egusphere-2024-3719
Preprint. Discussion started: 13 December 2024

mol^{-1} in ozone (**Fig. 3**). Therefore, CO levels (<50 nmol mol^{-1}), along with RH, were also utilized in the following section to better distinguish stratospheric air masses even though the NH has higher CO levels than the SH.

3.2 Stratospheric ozone in the UTLS

As discussed earlier in the methodology, aircraft RH observations are more accurate than ozonesondes. Therefore, we tested several RH filters on the air masses, aiming to minimize the impact of the reported error of the Vaisala RS91 sensor within the UTLS and to minimize the inclusion of tropospheric air. The following discussion is based on a 20% RH filter, while results for 30% and 10% RH are shown in the Supplement **(Fig. S2 and S3)**. **Figure 4** depicts ozone boxplots and the corresponding observation numbers (in the 10-base logarithm) by pressure bins. It is worth noting that the lowest three pressure bins have less data, particularly the lowest obtained from aircraft sampling **(Fig. 4)**, which implies a lower representativity in higher pressure bins (i.e., lower altitudes). The same observation applies to the 230-220 bin (mid spring).

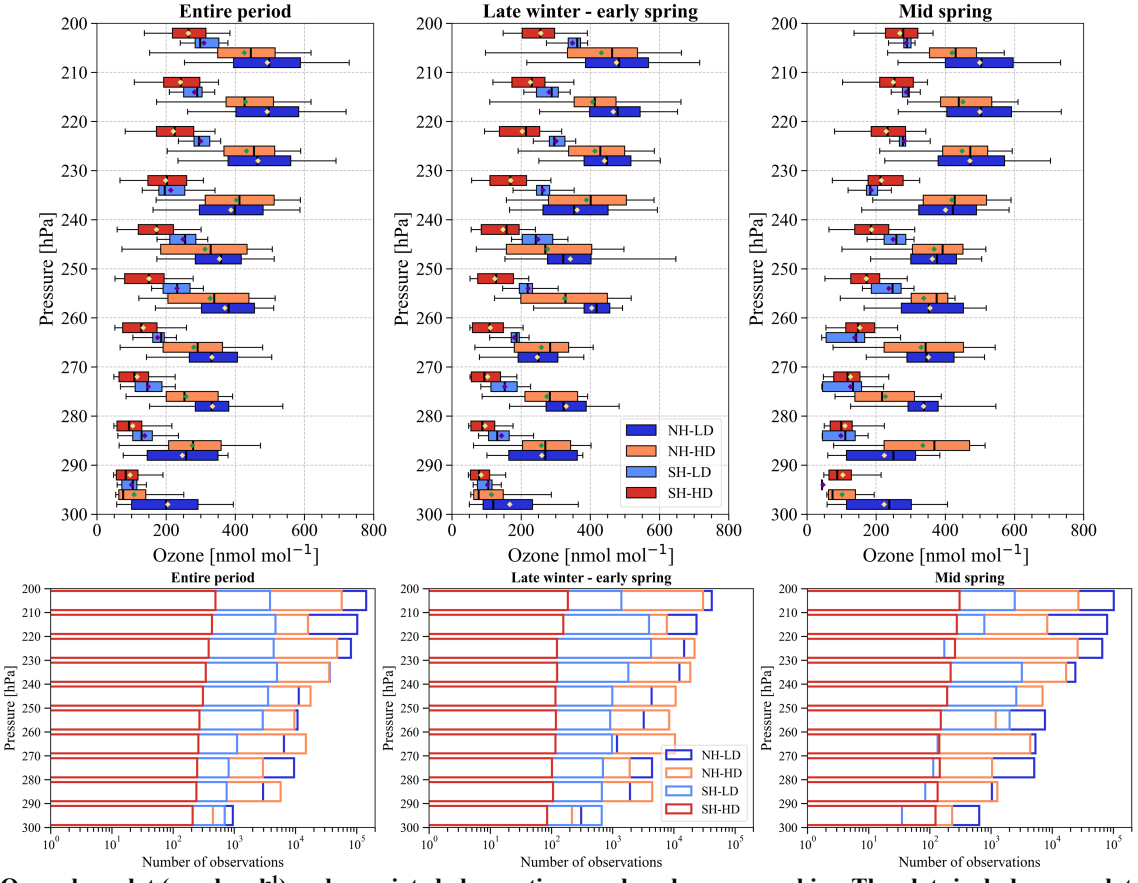

Figure 4: Ozone box plot (nmol mol^{-1}) and associated observation numbers by pressure bins. The plots include ozone data with RH lower than 20%. In the upper panel, the left, middle and right plots show the entire period, late winter-early spring and mid-spring respectively, for the northern and southern hemispheres and high-depleted and low-depleted years. Box plots indicate the median, the 25th and 75th percentiles. The whiskers extend to the 5th and 95th percentiles. In the lower panels, the X-axis shows the

https://doi.org/10.5194/egusphere-2024-3719
Preprint. Discussion started: 13 December 2024

observation numbers. The rest of the plot information is the same as described in the upper panel. High-depletion years in SH are based on ozonesondes launched from Ushuaia.

We observed higher ozone abundances in the NH for the entire period analyzed and for both subperiods, i.e., late winter-early spring and mid-spring compared with the SH (**Fig. 4**). We also noticed differences between high and low-depletion years, particularly in the SH, where this difference is more evident. In turn, the difference between low and high depletion years in the NH starts being visible at pressures less than 230 hPa (lower stratosphere).

In the SH, the ozone gap between high and low-depletion years was more intense in late winter-early spring, especially for pressures less than 270 hPa. Within this range (270-200 hPa), the difference between medians averaged 85 ± 15 nmol mol^{-1}, being on average 47% greater relative to high depletion years. While, in mid-spring, when depleted air from higher latitudes is expected to fully arrive over the study area, the gap in ozone was less, mainly at the range of 250-240 hPa, with a median of 74 ± 1 nmol mol^{-1}, and at 220-210 hPa with medians averaging 43 ± 3 nmol mol^{-1} (**Fig. 4**).

The higher ozone levels observed in the late winter-early spring of 2019 in the SH between 45º-60ºS compared to the reference period obtained from the ozonesondes (2008-2018) clearly illustrate the impact of the early polar vortex breakdown in September 2019 caused by the SSW event. In this region, Antarctic ozone depletion, more intense between 12 and 20 km, typically begins in August, accelerates in September, and reaches a minimum in October when ozone starts to recover. Therefore, the period of higher ozone destruction rate in September was entirely captured by the SouthTRAC mission.

Although the magnitude of the SSW event was not categorized as a major event, i.e., easterly winds did not reverse at 10 hPa at 60º S, it was strong enough to decrease the halogen-catalyzed ozone loss over the polar region and be detected in subpolar regions as shown in **Figure 4**. Later, in mid-spring, the observed ozone changes were less intense. Nonetheless, it is worth noting that even during this less ozone-depleted atypical scenario in 2019, the ozone abundance in the UTLS was not comparable to the higher levels observed in the NH, representing only 57% of the NH ozone median.

The agreement between CO and 20% RH filters varies with pressure bins, with a better agreement at pressures less than 270 hPa and where more aircraft measurements were achieved. On average, between 270 and 200 hPa, the percentage difference between both filters was 11 ± 8% in low depletion years (NH), 22 ± 17% in high depletion years (NH) and 4 ± 4% in low depletion years (SH). Thereby, **Figure B1** shows the ozone abundances by pressure bins after applying the carbon monoxide filter (<50 nmol mol-1). Similarly to the 20% RH filter, less ozone abundances were observed in the SH during low-depletion years compared with the NH. In the NH, differences between both subperiods can be noticed only in mid-spring at pressures less than 230 hPa.

We compared the ozone filtered by 20% RH in the UTLS obtained from SouthTRAC data over the study area with the entire longitudinal band calculated from the CAMS reanalysis. **Figure 5** shows that the reanalysis reproduces the interhemispheric differences and the interannual variability associated with high and low ozone depletion years. Also, the ozone medians obtained from the CAMS reanalysis and SouthTRAC are better matched for the late winter-early spring period, especially for

https://doi.org/10.5194/egusphere-2024-3719
Preprint. Discussion started: 13 December 2024

pressures below 270 hPa. In contrast, we observed higher fluctuations in the medians corresponding to the mid-spring period. These differences can be explained, in part, due to the lower flight frequency in this period, i.e., six flights during the mid-spring period versus ten in the late winter-early spring period.

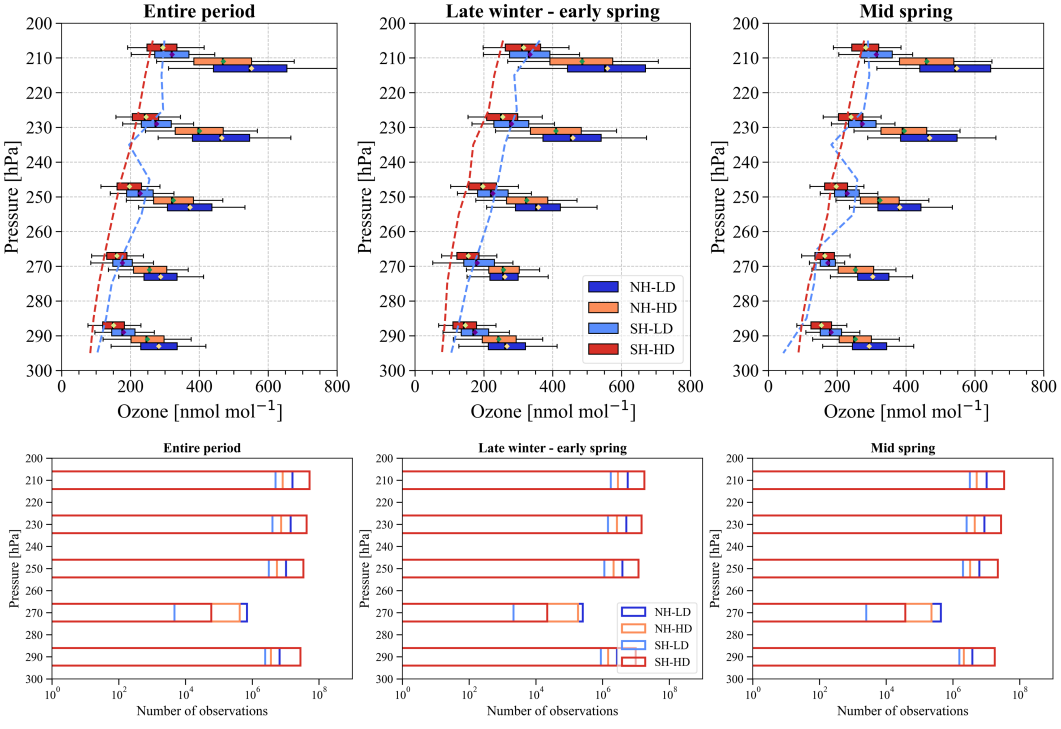

Figure 5: Ozone box plot (nmol mol^{-1}) and associated observation numbers by pressure bins obtained from CAMS reanalysis. The plots include ozone data with RH lower than 20%. The vertical red and blue dashed lines are the ozone medians in the SH obtained from ozonesondes (high depletion years) and SouthTRAC measurements (low depletion years), respectively. In the upper panel, the left, middle and right plots show the entire period, late winter-early spring and mid-spring, respectively, for the northern and southern hemispheres and high-depleted and low-depleted years. Box plots indicate the median, the 25th and 75th percentiles. The whiskers extend to the 5th and 95th percentiles. In the lower panels, the X-axis shows the observation numbers. The rest of the plot information is the same as described in the upper panel.

We delve into the apparent overestimation of ozone vertical gradient and medians obtained from the CAMS reanalysis across the entire longitudinal band of the Southern Hemisphere for high depletion years compared to ozonesonde measurements from the period 2008–2018 (**Fig. 6**). Consistently, the spatial distribution of ozone median (filtered by 20% RH) in the UTLS obtained by CAMS also shows lower levels over the SouthTRAC study area compared to much of the rest of the band (**Fig. 6**), suggesting that this overestimation may reflect ozone asymmetries in the UTLS over certain regions, as previously reported (Škerlak et al., 2014).

In **Fig. C1 in Appendix C**, we compare the identical study area for SouthTRAc and CAMS reanalysis. We observed a slight improvement for high ozone depletion years. Nevertheless, the ozone agreement in low depletion years worsens, showing an underestimation of CAMS reanalysis now.

https://doi.org/10.5194/egusphere-2024-3719
Preprint. Discussion started: 13 December 2024

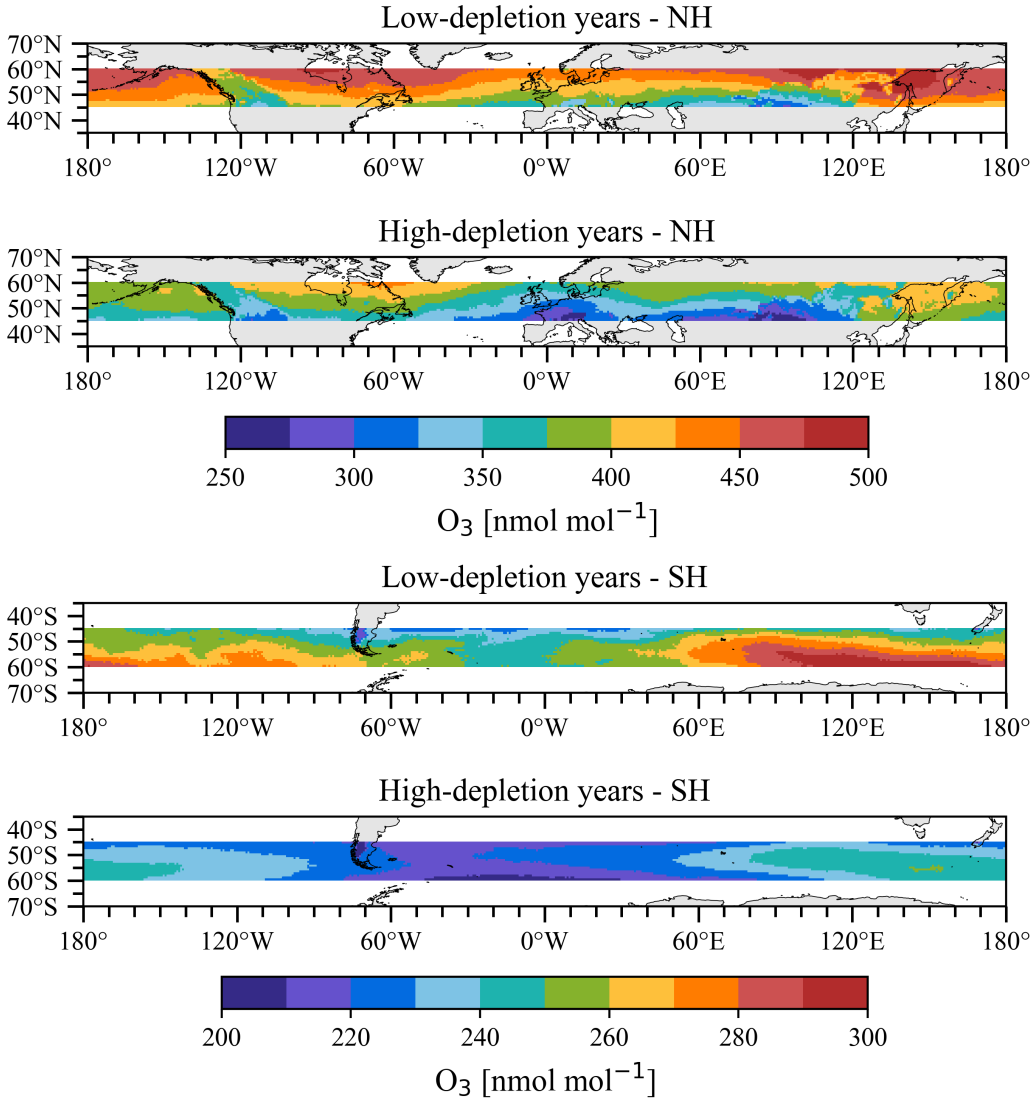

290

Figure 6: Ozone (nmol mol^{-1}) obtained from CAMS reanalysis filtered by RH lower than 20% and at a resolution of 0.75º x 0.75º. The upper panel depicts the ozone median in UTLS of the northern hemisphere, separated into low and high depletion years (entire period), while the lower panel describes the same for the southern hemispheres. Note that the scale of the color pallets are different in the NH and SH given the strong differences in ozone mixing ratios.

https://doi.org/10.5194/egusphere-2024-3719
Preprint. Discussion started: 13 December 2024

Conclusions

Tracer-to-tracer scatterplots between stratospheric ozone and tropospheric tracers (carbon monoxide and water vapor) are consistent with previous airborne campaign studies, which show high ozone and low carbon monoxide levels in the Southern Hemisphere (SH) in both the free troposphere and the upper troposphere-lower stratosphere (UTLS).

The bidirectional exchange observed in the UTLS during the 12 Nov flight provides evidence that transport from tropospheric sources can also influence this region of the atmosphere. During this flight, low levels of nitric acid (<500 pmol mol^{-1}) and hydrogen chloride (<50 pmol mol^{-1}) were consistently measured, alongside higher levels of carbon monoxide (>200 nmol mol^{-1}) and elevated water vapor (>100 μmol mol^{-1}), indicating a strong tropospheric signature in the UTLS.

The comparative analysis of ozone mixing ratios, characterized by stratospheric origin, shows lower levels in the SH UTLS (between 300-200 hPa and 45-60° latitude) compared with the Northern Hemisphere (NH). In high ozone depletion years, according to the stratospheric vortex, the ozone median in SH UTLS was 51% of that in the NH UTLS. During years impacted by early stratospheric sudden warming, i.e., low ozone depletion years, SH UTLS ozone median was 57% of the NH UTLS values. According to this characterization, we inferred that SH stratospheric intrusions have less ozone compared with the NH intrusions. Also, this lower ozone abundance in the SH was relatively proportional to the greater stratospheric ozone depletion observed in southern mid-and high latitudes.

We also found different ozone sensitivity to SSW in the UTLS of both hemispheres, being stronger in the SH than in the NH. In the SH, the impact of SSW was more evident during the late winter–early spring period, when the ozone difference was 47% higher compared with high-depletion years. This effect was less pronounced in the NH, becoming noticeable at pressures below 230 hPa, where the difference reached 10% between 4 Mar-20 May (8% in late winter-early spring). This difference was 7% for air masses filtered by carbon monoxide.

CAMS reproduced the ozone interhemispheric differences and the interannual variability associated with high and low ozone depletion years. The spatial comparison based on CAMS during high ozone depletion years also identified regions in the SH where the UTLS was poorer in ozone, with Patagonia being one such area. However, comparisons with in situ measurements showed important differences that must be reconciled.

Finally, two methodological aspects of this study should be considered when interpreting these comparisons. First, stratospheric air was characterized using relative humidity (RH) and carbon monoxide thresholds, aiming to exploit the in situ dataset rather than relying on modeling or potential vorticity. Second, differences in temporal and spatial coverage between the in situ measurements in the two hemispheres may affect the representativeness of the results at some pressure bins and periods.

https://doi.org/10.5194/egusphere-2024-3719
Preprint. Discussion started: 13 December 2024

Overall, this study emphasizes the need to expand highly resolved ozone profiles in the upper troposphere and lower stratosphere, particularly across the Southern Hemisphere where these measurements are crucial for accurately quantifying current stratosphere-troposphere exchange processes and their impact on the tropospheric ozone budget.

Appendix A: Tracer-to-tracer scatterplots between stratospheric tracers (nitric acid and hydrogen chloride) and ozone and carbon monoxide

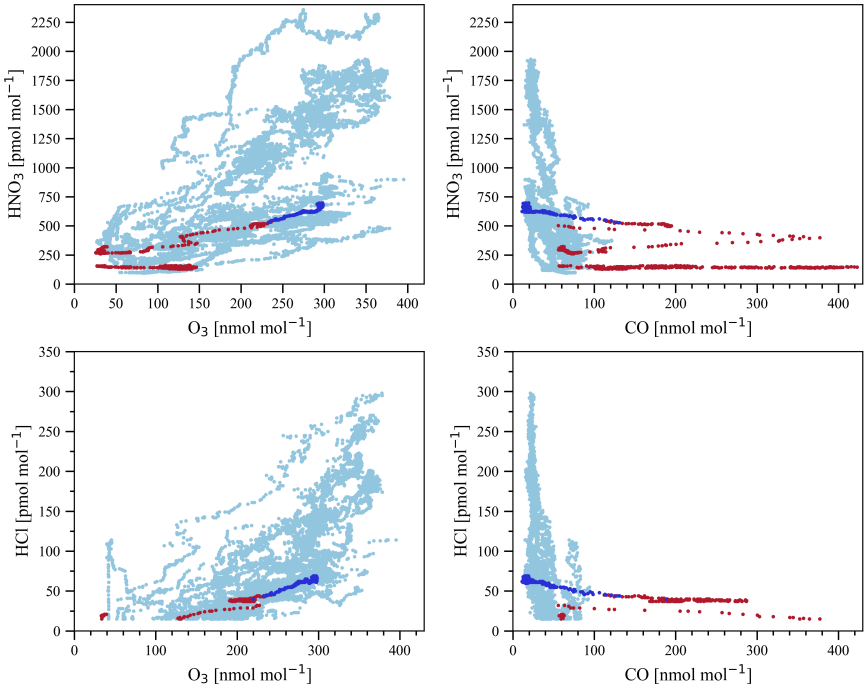

Figure A1: Scatter plots of nitric acid versus ozone, nitric acid versus carbon monoxide, hydrogen chloride versus ozone and hydrogen chloride versus carbon monoxide. Measurements obtained during the flight conducted on 12 Nov 2019 (ST25) are highlighted from the other flight measurements depending on their relative humidity in blue (< 20%) or in red (> 20%).

https://doi.org/10.5194/egusphere-2024-3719
Preprint. Discussion started: 13 December 2024

Appendix B: Air masses filtered by carbon monoxide

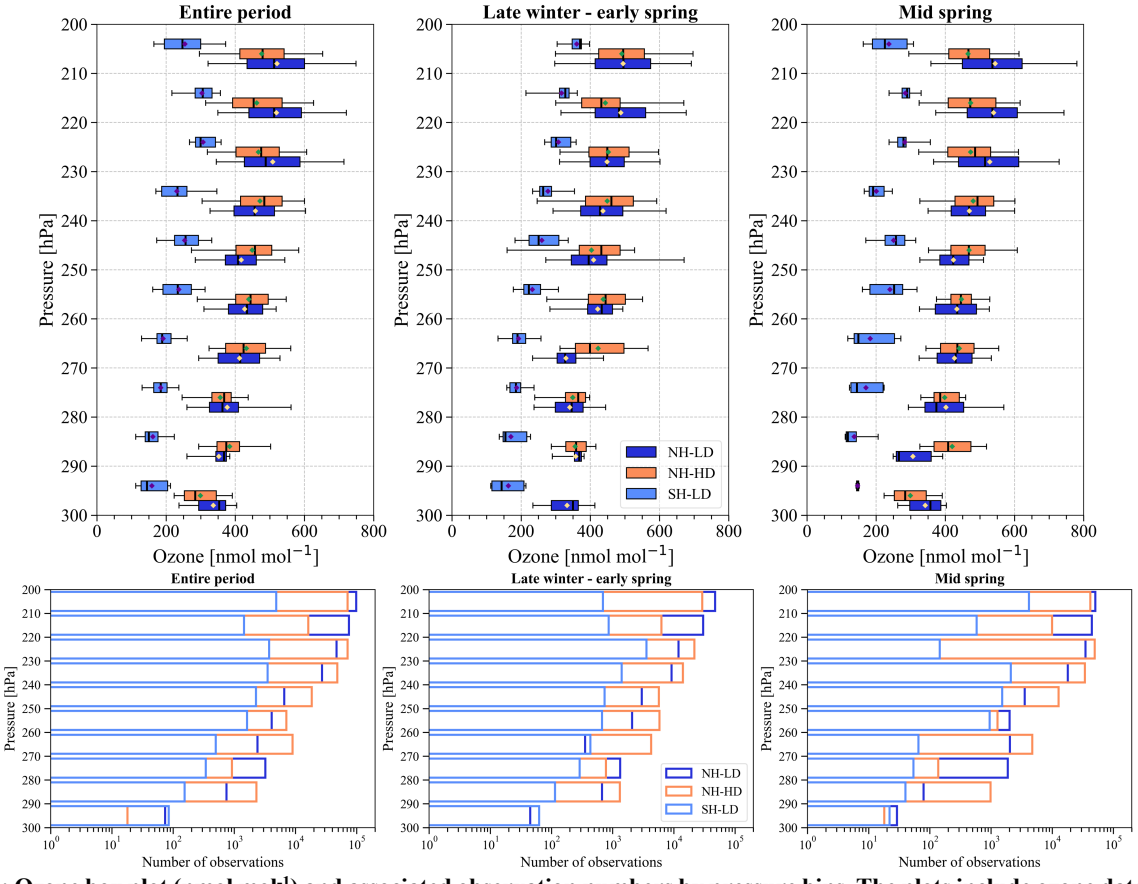

Figure B1: Ozone box plot (nmol mol^{-1}) and associated observation numbers by pressure bins. The plots include ozone data with CO lower than 50 nmol mol^{-1}. In the upper panel, the left, middle and right plots show the entire period, late winter-early spring and mid-spring for the northern and southern hemispheres and high-depleted and low-depleted years. Box plots indicate the median, the 25th and 75th percentiles. The whiskers extend to the 5th and 95th percentiles. In the lower panels, the X-axis shows the observation numbers. The rest of the plot information is the same as described in the upper panel.

https://doi.org/10.5194/egusphere-2024-3719
Preprint. Discussion started: 13 December 2024

Appendix C: Ozone comparison obtained from in situ measurements and CAMS reanalysis over the identical area (45º-60ºS and 90º-40º W)

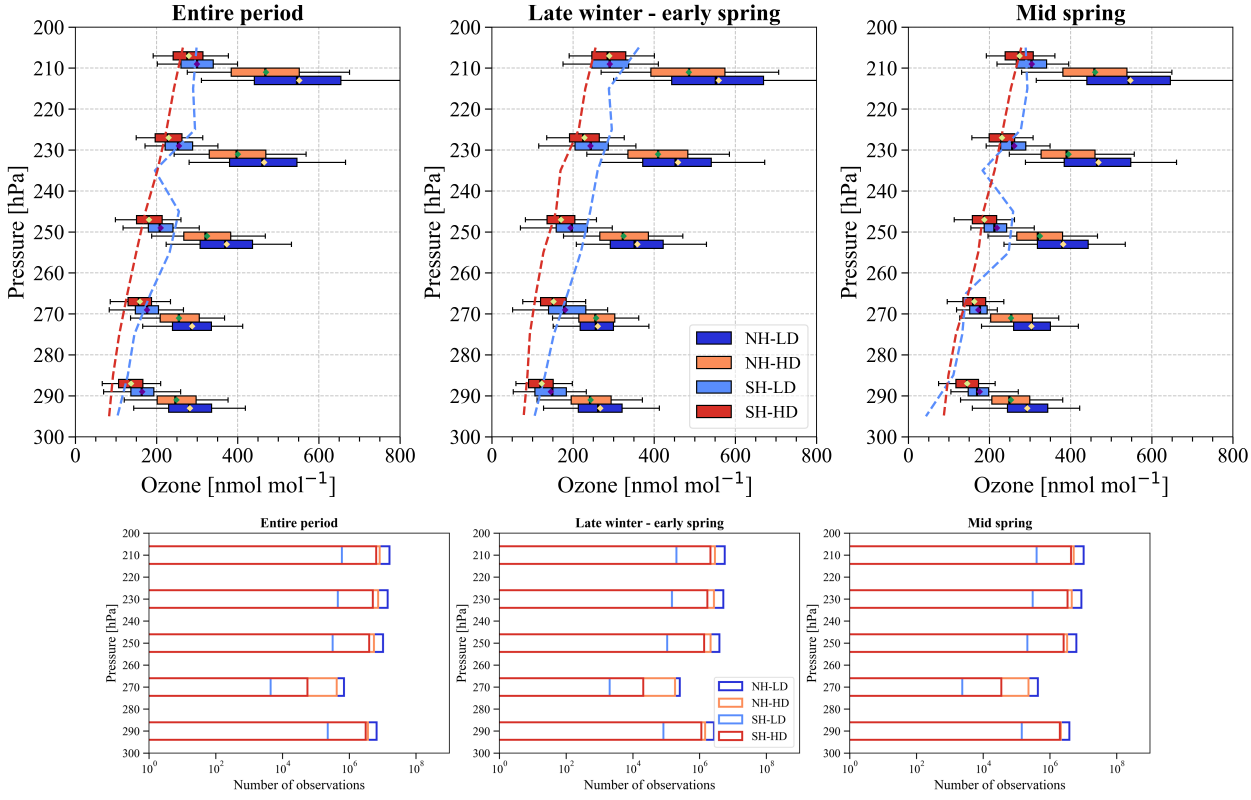

Figure C1: Ozone box plot (nmol mol^{-1}) and associated observation numbers by pressure bins obtained from CAMS reanalysis (45º-60ºS and 90º-40º W). The plots include ozone data with RH lower than 20%. The vertical red and blue dashed lines are the ozone medians in the SH obtained from ozonesondes (high depletion years) and SouthTRAC measurements (low depletion years), respectively. In the upper panel, the left, middle and right plots show the entire period, late winter-early spring and mid-spring, respectively, for the northern and southern hemispheres and high-depleted and low-depleted years. Box plots indicate the median, the 25th and 75th percentiles. The whiskers extend to the 5th and 95th percentiles. In the lower panels, the X-axis shows the observation numbers. The rest of the plot information is the same as described in the upper panel.

https://doi.org/10.5194/egusphere-2024-3719
Preprint. Discussion started: 13 December 2024

Data availability. SouthTRAC data can be accessed via the HALO database under https://halo-db.pa.op.dlr.de. IAGOS-CARIBIC data can be retrieved at https://zenodo.org/doi/10.5281/zenodo.8188548 (IAGOS-CORE / MOZAIC can be quoted via IAGOS-DB) (Zahn et al., 2024). Ozonesonde data for Ushuaia station can be retrieved from the World Ozone and Ultraviolet Radiation Data Centre (WOUDC) at http://woudc.org/archive/Archive-NewFormat/OzoneSonde_1.0_1/stn339/ecc (WOUDC, 2024).

Author contribution. RS, OC, YC, & CO: conceptualization. OC, CO, YC & RS: methodology. CO & YC: data curation. RS, CO, YC, & OC: formal analysis. RS: writing - original draft preparation. All authors: writing – review & editing. BS & PH initiated and coordinated the SouthTRAC campaign with the HALO research aircraft.

Competing interest. The contact author has declared that none of the authors has any competing interests.

Special issue statement. This article is part of the special issue "Tropospheric Ozone Assessment Report Phase II (TOAR-II) Community Special Issue (ACP/AMT/BG/GMD inter-journal SI)". It is a result of the Tropospheric Ozone Assessment Report, Phase II (TOAR-II, 2020–2024).

Acknowledgments. The authors acknowledge the collaboration provided by the Center for Climate and Resilience Research for the analysis contained in this article (ANID/FONDAP/1523A0002), the supercomputing infrastructure of the NLHPC (ECM-02). The authors thank the pilots, engineers, and scientists from DLR Flight Experiments for their excellent support during the SouthTRAC mission. The authors thank the following SouthTRAC members: Martin Zoeger (BAHAMAS data), Andreas Marsing (AIMS data) and Peter Hoor (CO data). The authors acknowledge that MOZAIC/CARIBIC/IAGOS data were created with support from the European Commission, national agencies in Germany (BMBF), France (MESR), and the UK (NERC), and the IAGOS member institutions (http://www.iagos.org/partners). The participating airlines (Lufthansa, Air France, Austrian, China Airlines, Hawaiian Airlines, Air Canada, Iberia, Eurowings Discover, Cathay Pacific, Air Namibia, Sabena) supported IAGOS by carrying the measurement equipment free of charge since 1994. The data are available at http://www.iagos.fr thanks to additional support from AERIS.

Financial support. This research has been partially supported by ANID (National Agency for Research and Development of Chile, grant no. ANID/FONDAP/1523A0002); ANID-DFG/FONDEQUIP-SouthTRAC/DFG190003; ANID/FONDECYT/1241459. JGU acknowledges funding by the German Science Foundation (Deutsche Forschungsgemeinschaft, DFG) Priority Program SPP 1294: HO4225/15-1, and HO4225/14-1

References

Archibald, A. T., Neu, J. L., Elshorbany, Y. F., Cooper, O. R., Young, P. J., Akiyoshi, H., Cox, R. A., Coyle, M., Derwent, R. G., Deushi, M., Finco, A., Frost, G. J., Galbally, I. E., Gerosa, G., Granier, C., Griffiths, P. T., Hossaini, R., Hu, L., Jöckel, P., Josse, B., Lin, M. Y., Mertens, M., Morgenstern, O., Naja, M., Naik, V., Oltmans, S., Plummer, D. A., Revell, L. E.,

https://doi.org/10.5194/egusphere-2024-3719
Preprint. Discussion started: 13 December 2024

Saiz-Lopez, A., Saxena, P., Shin, Y. M., Shahid, I., Shallcross, D., Tilmes, S., Trickl, T., Wallington, T. J., Wang, T., Worden, H. M., and Zeng, G.: Tropospheric ozone assessment report: A critical review of changes in the tropospheric ozone burden and budget from 1850 to 2100, https://doi.org/10.1525/elementa.2020.034, 2020.

Atkinson, R.: Atmospheric chemistry of VOCs and NO(x), Atmos Environ, 34, https://doi.org/10.1016/S1352-2310(99)00460-4, 2000.

Bourgeois, I., Peischl, J., Thompson, C. R., Aikin, K. C., Campos, T., Clark, H., Commane, R., Daube, B., Diskin, G. W., Elkins, J. W., Gao, R. S., Gaudel, A., Hintsa, E. J., Johnson, B. J., Kivi, R., McKain, K., Moore, F. L., Parrish, D. D., Querel, R., Ray, E., Sánchez, R., Sweeney, C., Tarasick, D. W., Thompson, A. M., Thouret, V., Witte, J. C., Wofsy, S. C., and Ryerson, T. B.: Global-scale distribution of ozone in the remote troposphere from the ATom and HIPPO airborne field missions, Atmos Chem Phys, 20, https://doi.org/10.5194/acp-20-10611-2020, 2020.

Brenninkmeijer, C. A. M., Crutzen, P. J., Fischer, H., Güsten, H., Hans, W., Heinrich, G., Heintzenberg, J., Hermann, M., Immelmann, T., Kersting, D., Maiss, M., Nolle, M., Pitscheider, A., Pohlkamp, H., Scharffe, D., Specht, K., and Wiedensohler, A.: CARIBIC-Civil Aircraft for global measurement of trace gases and aerosols in the tropopause region, J Atmos Ocean Technol, 16, https://doi.org/10.1175/1520-0426(1999)016<1373:CCAFGM>2.0.CO;2, 1999.

Brenninkmeijer, C. A. M., Crutzen, P., Boumard, F., Dauer, T., Dix, B., Ebinghaus, R., Filippi, D., Fischer, H., Franke, H., Frieß, U., Heintzenberg, J., Helleis, F., Hermann, M., Kock, H. H., Koeppel, C., Lelieveld, J., Leuenberger, M., Martinsson, B. G., Miemczyk, S., Moret, H. P., Nguyen, H. N., Nyfeler, P., Oram, D., O'Sullivan, D., Penkett, S., Platt, U., Pupek, M., Ramonet, M., Randa, B., Reichelt, M., Rhee, T. S., Rohwer, J., Rosenfeld, K., Scharffe, D., Schlager, H., Schumann, U., Slemr, F., Sprung, D., Stock, P., Thaler, R., Valentino, F., Van Velthoven, P., Waibel, A., Wandel, A., Waschitschek, K., Wiedensohler, A., Xueref-Remy, I., Zahn, A., Zech, U., and Ziereis, H.: Civil Aircraft for the regular investigation of the atmosphere based on an instrumented container: The new CARIBIC system, Atmos Chem Phys, 7, https://doi.org/10.5194/acp-7-4953-2007, 2007.

Butchart, N.: The Brewer-Dobson circulation, https://doi.org/10.1002/2013RG000448, 2014.

Clifton, O. E., Fiore, A. M., Massman, W. J., Baublitz, C. B., Coyle, M., Emberson, L., Fares, S., Farmer, D. K., Gentine, P., Gerosa, G., Guenther, A. B., Helmig, D., Lombardozzi, D. L., Munger, J. W., Patton, E. G., Pusede, S. E., Schwede, D. B., Silva, S. J., Sörgel, M., Steiner, A. L., and Tai, A. P. K.: Dry Deposition of Ozone Over Land: Processes, Measurement, and Modeling, https://doi.org/10.1029/2019RG000670, 2020.

Cooper, O., Forster, C., Parrish, D., Dunlea, E., Hübler, G., Fehsenfeld, F., Holloway, J., Oltmans, S., Johnson, B., Wimmers, A., and Horowitz, L.: On the life cycle of a stratospheric intrusion and its dispersion into polluted warm conveyor belts, Journal of Geophysical Research D: Atmospheres, 109, https://doi.org/10.1029/2003JD004006, 2004.

Dunn, R. J. H., D. M. Stanitski, N. Gobron, and K. M. Willett, Eds., 2020: Global Climate [in "State of the Climate in 2019"]. *Bull. Amer. Meteor.*, 101 (8), S9–S127, https://doi.org/10.1175/BAMS- D-20-0104.1.

Dunn, R. J. H., J. B Miller, K. M. Willett, and N. Gobron, Eds., 2023: Global Climate [in "State of the Climate in 2022"]. Bull. Amer. Meteor. Soc., 104 (9), S11–S145, https://doi.org/10.1175/BAMS-D-23-0090.1.

https://doi.org/10.5194/egusphere-2024-3719
Preprint. Discussion started: 13 December 2024

Dyroff, C., Zahn, A., Christner, E., Forbes, R., Tompkins, A. M., and van Velthoven, P. F. J.: Comparison of ECMWF analysis and forecast humidity data with CARIBIC upper troposphere and lower stratosphere observations, Quarterly Journal of the Royal Meteorological Society, 141, https://doi.org/10.1002/qj.2400, 2015.

Ermel, M., Oswald, R., Mayer, J. C., Moravek, A., Song, G., Beck, M., Meixner, F. X., and Trebs, I.: Preparation methods to optimize the performance of sensor discs for fast chemiluminescence ozone analyzers, Environ Sci Technol, 47, https://doi.org/10.1021/es3040363, 2013.

Forster, P., T. Storelvmo, K. Armour, W. Collins, J.-L. Dufresne, D. Frame, D.J. Lunt, T. Mauritsen, M.D. Palmer, M. Watanabe, M. Wild, and H. Zhang, 2021: The Earth's Energy Budget, Climate Feedbacks, and Climate Sensitivity. In *Climate Change 2021: The Physical Science Basis. Contribution of Working Group I to the Sixth Assessment Report of the Intergovernmental Panel on Climate Change* [Masson-Delmotte, V., P. Zhai, A. Pirani, S.L. Connors, C. Péan, S. Berger, N. Caud, Y. Chen, L. Goldfarb, M.I. Gomis, M. Huang, K. Leitzell, E. Lonnoy, J.B.R. Matthews, T.K. Maycock, T. Waterfield, O. Yelekçi, R. Yu, and B. Zhou (eds.)]. Cambridge University Press, Cambridge, United Kingdom and New York, NY, USA, pp. 923–1054, doi:10.1017/9781009157896.009.

Garfinkel, C. I., Aquila, V., Waugh, D. W., and Oman, L. D.: Time-varying changes in the simulated structure of the Brewer-Dobson Circulation, Atmos Chem Phys, 17, https://doi.org/10.5194/acp-17-1313-2017, 2017.

Gettelman, a., Pan, L. L., Randel, W. J., Hoor, P., Birner, T., and Hegglin, M. I.: the Extratropical Upper Troposphere and Lower Stratosphere, Reviews of Geophysics, 49, https://doi.org/10.1029/2011RG000355.1.INTRODUCTION, 2011.

Giez, A., Mallaun, C., Zöger, M., Dörnbrack, A., and Schumann, U.: Static pressure from aircraft trailing-cone measurements and numerical weather-prediction analysis, J Aircr, 54, https://doi.org/10.2514/1.C034084, 2017.

Griffiths, P. T., Murray, L. T., Zeng, G., Shin, Y. M., Abraham, N. L., Archibald, A. T., Deushi, M., Emmons, L. K., Galbally, I. E., Hassler, B., Horowitz, L. W., Keeble, J., Liu, J., Moeini, O., Naik, V., O'Connor, F. M., Oshima, N., Tarasick, D., Tilmes, S., Turnock, S. T., Wild, O., Young, P. J., and Zanis, P.: Tropospheric ozone in CMIP6 simulations, Atmos Chem Phys, 21, https://doi.org/10.5194/acp-21-4187-2021, 2021.

Health Effects Institute: State of Global Air 2020. Special Report, MA:Health Effects Instiute, 2020.

Helten, M., Smit, H. G. J., Sträter, W., Kley, D., Nedelec, P., Zöger, M., and Busen, R.: Calibration and performance of automatic compact instrumentation for the measurement of relative humidity from passenger aircraft, Journal of Geophysical Research Atmospheres, 103, https://doi.org/10.1029/98JD00536, 1998.

Inness, A., Ades, M., Agustí-Panareda, A., Barr, J., Benedictow, A., Blechschmidt, A. M., Jose Dominguez, J., Engelen, R., Eskes, H., Flemming, J., Huijnen, V., Jones, L., Kipling, Z., Massart, S., Parrington, M., Peuch, V. H., Razinger, M., Remy, S., Schulz, M., and Suttie, M.: The CAMS reanalysis of atmospheric composition, Atmos Chem Phys, 19, https://doi.org/10.5194/acp-19-3515-2019, 2019.

Jensen, M. P., Holdridge, D. J., Survo, P., Lehtinen, R., Baxter, S., Toto, T., and Johnson, K. L.: Comparison of Vaisala radiosondes RS41 and RS92 at the ARM Southern Great Plains site, Atmos. Meas. Tech., 9, 3115–3129, https://doi.org/10.5194/amt-9-3115-2016, 2016

https://doi.org/10.5194/egusphere-2024-3719
Preprint. Discussion started: 13 December 2024

Johansson, S., Wetzel, G., Friedl-Vallon, F., Glatthor, N., Höpfner, M., Kleinert, A., Neubert, T., Sinnhuber, B.-M., and Ungermann, J.: Biomass burning pollution in the South Atlantic upper troposphere: GLORIA trace gas observations and evaluation of the CAMS model, Atmos. Chem. Phys., 22, 3675–3691, https://doi.org/10.5194/acp-22-3675-2022, 2022

Jurkat, T., Kaufmann, S., Voigt, C., Schäuble, D., Jeßberger, P., and Ziereis, H.: The airborne mass spectrometer AIMS - Part 2: Measurements of trace gases with stratospheric or tropospheric origin in the UTLS, Atmos Meas Tech, 9, https://doi.org/10.5194/amt-9-1907-2016, 2016.

Kaufmann, S., Voigt, C., Heller, R., Jurkat-Witschas, T., Krämer, M., Rolf, C., Zöger, M., Giez, A., Buchholz, B., Ebert, V., Thornberry, T., and Schumann, U.: Intercomparison of midlatitude tropospheric and lower-stratospheric water vapor measurements and comparison to ECMWF humidity data, Atmos Chem Phys, 18, https://doi.org/10.5194/acp-18-16729-2018, 2018.

Kloss, C., Sellitto, P., von Hobe, M., Berthet, G., Smale, D., Krysztofiak, G., Xue, C., Qiu, C., Jégou, F., Ouerghemmi, I., and Legras, B.: Australian Fires 2019–2020: Tropospheric and Stratospheric Pollution Throughout the Whole Fire Season, Front Environ Sci, 9, https://doi.org/10.3389/fenvs.2021.652024, 2021.

Lu, X., Zhang, L., Zhao, Y., Jacob, D. J., Hu, Y., Hu, L., Gao, M., Liu, X., Petropavlovskikh, I., McClure-Begley, A., and Querel, R.: Surface and tropospheric ozone trends in the Southern Hemisphere since 1990: possible linkages to poleward expansion of the Hadley circulation, Sci Bull (Beijing), 64, https://doi.org/10.1016/j.scib.2018.12.021, 2019.

Marenco, A., Thouret, V., Nédélec, P., Smit, H., Helten, M., Kley, D., Karcher, F., Simon, P., Law, K., Pyle, J., Poschmann, G., Von Wrede, R., Hume, C., and Cook, T.: Measurement of ozone and water vapor by Airbus in-service aircraft: The MOZAIC airborne program, An overview, https://doi.org/10.1029/98JD00977, 1998.

McConnell, R., Berhane, K., Gilliland, F., London, S. J., Islam, T., Gauderman, W. J., Avol, E., Margolis, H. G., and Peters, J. M.: Asthma in exercising children exposed to ozone: A cohort study, Lancet, 359, https://doi.org/10.1016/S0140-6736(02)07597-9, 2002.

Monks, P. S., Archibald, A. T., Colette, A., Cooper, O., Coyle, M., Derwent, R., Fowler, D., Granier, C., Law, K. S., Mills, G. E., Stevenson, D. S., Tarasova, O., Thouret, V., Von Schneidemesser, E., Sommariva, R., Wild, O., and Williams, M. L.: Tropospheric ozone and its precursors from the urban to the global scale from air quality to short-lived climate forcer, https://doi.org/10.5194/acp-15-8889-2015, 2015.

Müller, S., Hoor, P., Berkes, F., Bozem, H., Klingebiel, M., Reutter, P., Smit, H. G. J., Wendisch, M., Spichtinger, P., and Borrmann, S.: In situ detection of stratosphere-troposphere exchange of cirrus particles in the midlatitudes, Geophys Res Lett, 42, https://doi.org/10.1002/2014GL062556, 2015.

Nédélec, P., Blot, R., Boulanger, D., Athier, G., Cousin, J. M., Gautron, B., Petzold, A., Volz-Thomas, A., and Thouret, V.: Instrumentation on commercial aircraft for monitoring the atmospheric composition on a global scale: The IAGOS system, technical overview of ozone and carbon monoxide measurements, Tellus B Chem Phys Meteorol, 6, https://doi.org/10.3402/tellusb.v67.27791, 2015.

https://doi.org/10.5194/egusphere-2024-3719
Preprint. Discussion started: 13 December 2024

Nedelec, P., Cammas, J. P., Thouret, V., Athier, G., Cousin, J. M., Legrand, C., Abonnel, C., Lecoeur, F., Cayez, G., and Marizy, C.: An improved infrared carbon monoxide analyser for routine measurements aboard commercial Airbus aircraft: Technical validation and first scientific results of the MOZAIC III programme, Atmos Chem Phys, 3, https://doi.org/10.5194/acp-3-1551-2003, 2003.

Neis, P., Smit, H. G. J., Rohs, S., Bundke, U., Krämer, M., Spelten, N., Ebert, V., Buchholz, B., Thomas, K., and Petzold, A.: Quality assessment of MOZAIC and IAGOS capacitive hygrometers: Insights from airborne field studies, Tellus B Chem Phys Meteorol, 6, https://doi.org/10.3402/tellusb.v67.28320, 2015.

Ohyama, H., Mizuno, A., Zamorano, F., Sugita, T., Akiyoshi, H., Noguchi, K., Wolfram, E., Salvador, J., and Benitez, G. C.: Characteristics of Atmospheric Wave-Induced Laminae Observed by Ozonesondes at the Southern Tip of South America, Journal of Geophysical Research: Atmospheres, 123, https://doi.org/10.1029/2018JD028707, 2018.

Petzold, A., Thouret, V., Gerbig, C., Zahn, A., Brenninkmeijer, C. A. M., Gallagher, M., Hermann, M., Pontaud, M., Ziereis, H., Boulanger, D., Marshall, J., NéDélec, P., Smit, H. G. J., Friess, U., Flaud, J. M., Wahner, A., Cammas, J. P., Volz-Thomas, A., Thomas, K., Rohs, S., Bundke, U., Neis, P., Berkes, F., Houben, N., Berg, M., Tappertzhofen, M., Blomel, T., Pätz, W., Filges, A., Boschetti, F., Verma, S., Baum, S., Athier, G., Cousin, J. M., Sauvage, B., Blot, R., Clark, H., Gaudel, A., Gressent, A., Auby, A., Fontaine, A., Gautron, B., Bennouna, Y., Petetin, H., Karcher, F., Abonnel, C., Dandin, P., Beswick, K., Wang, K. Y., Rauthe-Schöch, A., Baker, A. K., Riede, H., Gromov, S., Zimmermann, P., Thorenz, U., Scharffe, D., Koeppel, C., Slemr, F., Schuck, T. J., Umezawa, T., Ditas, J., Cheng, Y., Schneider, J., Williams, J., Neumaier, M., Christner, E., Fischbeck, G., Safadi, L., Petrelli, A., Gehrlein, T., Heger, S., Dyroff, C., Weber, S., Assmann, D., Rubach, F., Weigelt, A., Stratmann, G., Stock, P., Penth, L., Walter, D., Heue, K. P., Allouche, Y., Marizy, C., Hermira, J., Bringtown, S., Saueressig, G., Seidel, N., Huf, M., Waibel, A., Franke, H., Klaus, C., Stosius, R., Baumgardner, D., Braathen, G., Paulin, M., and Garnett, N.: Global-scale atmosphere monitoring by in-service aircraft - current achievements and future prospects of the European Research Infrastructure IAGOS, Tellus B Chem Phys Meteorol, 6, https://doi.org/10.3402/tellusb.v67.28452, 2015.

Rapp, M., Kaifler, B., Dörnbrack, A., Gisinger, S., Mixa, T., Reichert, R., Kaifler, N., Knobloch, S., Eckert, R., Wildmann, N., Giez, A., Krasauskas, L., Preusse, P., Geldenhuys, M., Riese, M., Woiwode, W., Friedl-Vallon, F., Sinnhuber, B. M., De la Torre, A., Alexander, P., Hormaechea, J. L., Janches, D., Garhammer, M., Chau, J. L., Federico Conte, J., Hoor, P., and Engel, A.: Southtrac-gw: An airborne field campaign to explore gravity wave dynamics at the world's strongest hotspot, Bull Am Meteorol Soc, 102, https://doi.org/10.1175/BAMS-D-20-0034.1, 2021.

Riese, M., Ploeger, F., Rap, A., Vogel, B., Konopka, P., Dameris, M., and Forster, P.: Impact of uncertainties in atmospheric mixing on simulated UTLS composition and related radiative effects, Journal of Geophysical Research Atmospheres, 117, https://doi.org/10.1029/2012JD017751, 2012.

Rolf, C., Afchine, A., Bozem, H., Buchholz, B., Ebert, V., Guggenmoser, T., Hoor, P., Konopka, P., Kretschmer, E., Müller, S., Schlager, H., Spelten, N., Sumiáska-Ebersoldt, O., Ungermann, J., Zahn, A., and Krämer, M.: Transport of Antarctic

https://doi.org/10.5194/egusphere-2024-3719
Preprint. Discussion started: 13 December 2024

stratospheric strongly dehydrated air into the troposphere observed during the HALO-ESMVal campaign 2012, Atmos Chem Phys, 15, https://doi.org/10.5194/acp-15-9143-2015, 2015.

Rolf, C., Rohs, S., Smit, H. G. J., Krämer, M., Bozóki, Z., Hofmann, S., Franke, H., Maser, R., Hoor, P., and Petzold, A.: Evaluation of compact hygrometers for continuous airborne measurements, Meteorologische Zeitschrift, 33, https://doi.org/10.1127/metz/2023/1187, 2024.

Saunois, M., R. Stavert, A., Poulter, B., Bousquet, P., G. Canadell, J., B. Jackson, R., A. Raymond, P., J. Dlugokencky, E., Houweling, S., K. Patra, P., Ciais, P., K. Arora, V., Bastviken, D., Bergamaschi, P., R. Blake, D., Brailsford, G., Bruhwiler, L., M. Carlson, K., Carrol, M., Castaldi, S., Chandra, N., Crevoisier, C., M. Crill, P., Covey, K., L. Curry, C., Etiope, G., Frankenberg, C., Gedney, N., I. Hegglin, M., Höglund-Isaksson, L., Hugelius, G., Ishizawa, M., Ito, A., Janssens-Maenhout, G., M. Jensen, K., Joos, F., Kleinen, T., B. Krummel, P., L. Langenfelds, R., G. Laruelle, G., Liu, L., MacHida, T., Maksyutov, S., C. McDonald, K., McNorton, J., A. Miller, P., R. Melton, J., Morino, I., Müller, J., Murguia-Flores, F., Naik, V., Niwa, Y., Noce, S., O'Doherty, S., J. Parker, R., Peng, C., Peng, S., P. Peters, G., Prigent, C., Prinn, R., Ramonet, M., Regnier, P., J. Riley, W., A. Rosentreter, J., Segers, A., J. Simpson, I., Shi, H., J. Smith, S., Paul Steele, L., F. Thornton, B., Tian, H., Tohjima, Y., N. Tubiello, F., Tsuruta, A., Viovy, N., Voulgarakis, A., S. Weber, T., Van Weele, M., R. Van Der Werf, G., F. Weiss, R., Worthy, D., Wunch, D., Yin, Y., Yoshida, Y., Zhang, W., Zhang, Z., Zhao, Y., Zheng, B., Zhu, Q., Zhu, Q., and Zhuang, Q.: The global methane budget 2000-2017, Earth Syst Sci Data, 12, https://doi.org/10.5194/essd-12-1561-2020, 2020.

Scambos, T. and Stammerjohn, and S.: State of the Climate in 2019. Antarctica and the Southern Ocean, Bulletin of the American Meteorological Society, 2020.

Scharffe, D., Slemr, F., Brenninkmeijer, C. A. M., and Zahn, A.: Carbon monoxide measurements onboard the CARIBIC passenger aircraft using UV resonance fluorescence, Atmos Meas Tech, 5, https://doi.org/10.5194/amt-5-1753-2012, 2012.

Skeie, R. B., Myhre, G., Hodnebrog, Ø., Cameron-Smith, P. J., Deushi, M., Hegglin, M. I., Horowitz, L. W., Kramer, R. J., Michou, M., Mills, M. J., Olivié, D. J. L., Connor, F. M. O., Paynter, D., Samset, B. H., Sellar, A., Shindell, D., Takemura, T., Tilmes, S., and Wu, T.: Historical total ozone radiative forcing derived from CMIP6 simulations, NPJ Clim Atmos Sci, 3, https://doi.org/10.1038/s41612-020-00131-0, 2020.

Škerlak, B., Sprenger, M., and Wernli, H.: A global climatology of stratosphere-troposphere exchange using the ERA-Interim data set from 1979 to 2011, Atmos Chem Phys, 14, https://doi.org/10.5194/acp-14-913-2014, 2014.

Smit, H. G. J., Rohs, S., Neis, P., Boulanger, D., Krämer, M., Wahner, A., and Petzold, A.: Technical note: Reanalysis of upper troposphere humidity data from the MOZAIC programme for the period 1994 to 2009, Atmos Chem Phys, 14, https://doi.org/10.5194/acp-14-13241-2014, 2014.

Stohl, A., Bonasoni, P., Cristofanelli, P., Collins, W., Feichter, J., Frank, A., Forster, C., Gerasopoulos, E., Gäggeler, H., James, P., Kentarchos, T., Kromp-Kolb, H., Krüger, B., Land, C., Meloen, J., Papayannis, A., Priller, A., Seibert, P., Sprenger, M., Roelofs, G. J., Scheel, H. E., Schnabel, C., Siegmund, P., Tobler, L., Trickl, T., Wernli, H., Wirth, V., Zanis,

https://doi.org/10.5194/egusphere-2024-3719
Preprint. Discussion started: 13 December 2024

P., and Zerefos, C.: Stratosphere-troposphere exchange: A review, and what we have learned from STACCATO, Journal of Geophysical Research Atmospheres, 108, https://doi.org/10.1029/2002jd002490, 2003.

Stratmann, G., Ziereis, H., Stock, P., Brenninkmeijer, C. A. M., Zahn, A., Rauthe-Schöch, A., Velthoven, P. V., Schlager, H., and Volz-Thomas, A.: NO and NOy in the upper troposphere: Nine years of CARIBIC measurements onboard a passenger aircraft, Atmos Environ, 133, https://doi.org/10.1016/j.atmosenv.2016.02.035, 2016.

Szopa, S., Naik, V., Adhikary, B., Artaxo, P., Berntsen, T., Collins, W.D., Fuzzi, S., Gallardo, L., Kiendler-Scharr, A., Klimont, Z., Liao, H., Unger, N., and Zanis, P.: Short-Lived Climate Forcers. In Climate Change 2021: The Physical Science Basis. Contribution of Working Group I to the Sixth Assessment Report of the Intergovernmental Panel on Climate Change [Masson-Delmotte, V., P. Zhai, A. Pirani, S.L. Connors, C. Péan, S. Berger, N. Caud, Y. Chen, L. Goldfarb, M.I. Gomis, M. Huang, K. Leitzell, E. Lonnoy, J.B.R. Matthews, T.K. Maycock, T. Waterfield, O. Yelekçi, R. Yu, and B. Zhou (eds.)]. Cambridge University Press, Cambridge, United Kingdom and New York, NY, USA, pp. 817–922, doi:10.1017/9781009157896.008, 2021

Thouret, V., Marenco, A., Logan, J. A., Nédélec, P., and Grouhel, C.: Comparisons of ozone measurements from the MOZAIC airborne program and the ozone sounding network at eight locations, https://doi.org/10.1029/98JD02243, 1998.

WOUDC, 2024: http://woudc.org/archive/Archive-NewFormat/OzoneSonde_1.0_1/stn339/ecc, last access: 31 July 2024

Zahn, A., Christner, E., Van Velthoven, P. F. J., Rauthe-Schöch, A., and Brenninkmeijer, C. A. M.: Processes controlling water vapor in the upper troposphere/lowermost stratosphere: An analysis of 8years of monthly measurements by the IAGOS-CARIBIC observatory, J Geophys Res, 119, https://doi.org/10.1002/2014JD021687, 2014.

Zahn, A., Obersteiner, F., Gehrlein, T., Neumaier, M., Dyroff, C., Förster, E., Sprung, D., Van Velthoven, P., Xueref-Remy, I., Ziereis, H., Bundke, U., Gerbig, C., Scharffe, D., Slemr, F., Weber, S., Hermann, M., Cheng, Y., & Bönisch, H. (2024). IAGOS-CARIBIC MS files collection (v2024.10.28) (2024.10.28) [Data set]. Zenodo: https://zenodo.org/doi/10.5281/zenodo.8188548, last access: 6 May 2023

Zahn, A., Weppner, J., Widmann, H., Schlote-Holubek, K., Burger, B., Kühner, T., and Franke, H.: A fast and precise chemiluminescence ozone detector for eddy flux and airborne application, Atmos Meas Tech, 5, https://doi.org/10.5194/amt-5-363-2012, 2012.

Zeng, G., Querel, R., Shiona, H., Poyraz, D., Van Malderen, R., Geddes, A., Smale, P., Smale, D., Robinson, J., and Morgenstern, O.: Analysis of a newly homogenised ozonesonde dataset from Lauder, New Zealand, Atmos. Chem. Phys., 24, 6413–6432, https://doi.org/10.5194/acp-24-6413-2024, 2024.

Zheng, X. yan, Orellano, P., Lin, H. liang, Jiang, M., and Guan, W. jie: Short-term exposure to ozone, nitrogen dioxide, and sulphur dioxide and emergency department visits and hospital admissions due to asthma: A systematic review and meta-analysis, Environ Int, 150, https://doi.org/10.1016/j.envint.2021.106435, 2021.